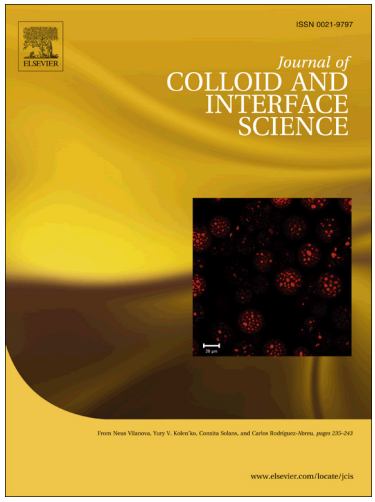

Aloe vera extract functionalized zinc oxide nanoparticles as nanoantibiotics against multi-drug resistant clinical bacterial isolates

Khursheed Alia, Sourabh Dwivedi, Ameer Azam, Quaiser Saquib, Mansour S. Al-Said, Abdulaziz A. Alkhedhairy, Javed Musarrat

PII: S0021-9797(16)30163-1
DOI: http://dx.doi.org/10.1016/j.jcis.2016.03.021
Reference: YJCIS 21145

To appear in: *Journal of Colloid and Interface Science*

Received Date: 22 December 2015
Revised Date: 9 March 2016
Accepted Date: 11 March 2016

Please cite this article as: K. Alia, S. Dwivedi, A. Azam, Q. Saquib, M.S. Al-Said, A.A. Alkhedhairy, J. Musarrat, *Aloe vera* extract functionalized zinc oxide nanoparticles as nanoantibiotics against multi-drug resistant clinical bacterial isolates, *Journal of Colloid and Interface Science* (2016), doi: http://dx.doi.org/10.1016/j.jcis.2016.03.021

Aloe vera extract functionalized zinc oxide nanoparticles as nanoantibiotics against multi-drug resistant clinical bacterial isolates

Khursheed Ali[a], Sourabh Dwivedi[a], Ameer Azam[b], Quaiser Saquib[c], Mansour S. Al-Said[d], Abdulaziz A. Alkhedhairy[c] and Javed Musarrat[a,e]

[a]Department of Agricultural Microbiology, Faculty of Agricultural Sciences, Aligarh Muslim University, Aligarh-202002, U.P., India

[b]Department of Applied Physics, Faculty of Engineering & Technology, Aligarh Muslim University, Aligarh- 202002, U.P., India.

[c]Chair for DNA Research, Department of Zoology, College of Science, King Saud University, P.O. Box 2455, Riyadh 11451, Saudi Arabia.

[d]Department of Pharmacognosy, College of Pharmacy, King Saud University, P.O. Box 2457, Riyadh 11451, Kingdom of Saudi Arabia

[e]Department of Biosciences and Biotechnology, BGSBU, Rajouri, J & K, India

Corresponding author:

Prof. Javed Musarrat

Department of Agricultural Microbiology

Faculty of Agricultural Sciences

Aligarh Muslim University

Aligarh 202002, U.P. India

Tel: +919760785651

Email: musarratj1@yahoo.com

Aloe vera extract functionalized zinc oxide nanoparticles as nanoantibiotics against multi-drug resistant clinical bacterial isolates

Khursheed Ali[a], Sourabh Dwivedi[a], Ameer Azam[b], Quaiser Saquib[c], Mansour S. Al-Said[d], Abdulaziz A. Alkhedhairy[c] and Javed Musarrat[a,e]

[a]Department of Agricultural Microbiology, Faculty of Agricultural Sciences, Aligarh Muslim University, Aligarh-202002, U.P., India

[b]Department of Applied Physics, Faculty of Engineering & Technology, Aligarh Muslim University, Aligarh- 202002, U.P., India.

[c]Chair for DNA Research, Department of Zoology, College of Science, King Saud University, P.O. Box 2455, Riyadh 11451, Saudi Arabia.

[d]Department of Pharmacognosy, College of Pharmacy, King Saud University, P.O. Box 2457, Riyadh 11451, Kingdom of Saudi Arabia

[e]Department of Biosciences and Biotechnology, BGSBU, Rajouri, J & K, India

Corresponding author:

Prof. Javed Musarrat

Department of Agricultural Microbiology

Faculty of Agricultural Sciences

Aligarh Muslim University

Aligarh 202002, U.P. India

Tel: +919760785651

Email: musarratj1@yahoo.com

Abstract

ZnO nanoparticles (ZnONPs) were synthesised through a simple and efficient biogenic synthesis approach, exploiting the reducing and capping potential of *Aloe barbadensis* Miller (*A. vera*) leaf extract (ALE). ALE-capped ZnO nanoparticles (ALE-ZnONPs) were characterized using UV-Vis spectroscopy, X-ray diffraction (XRD), Fourier transform infrared (FTIR) spectroscopy, scanning electron microscopy (SEM), energy dispersive X-ray spectroscopy (EDX), and transmission electron microscopy (TEM) analyses. XRD analysis provided the average size of ZnONPs as 15 nm. FTIR spectral analysis suggested the role of phenolic compounds, terpenoids and proteins present in ALE, in nucleation and stability of ZnONPs. Flow cytometry and atomic absorption spectrophotometry (AAS) data analyses revealed the surface binding and internalization of ZnONPs in Gram +ve (*S. aureus*) and Gram -ve (*E. coli*) cells, respectively. Significant antibacterial activity of ALE-ZnONPs was observed against extended spectrum beta lactamases (ESBL) positive *E. coli*, *P. aeruginosa*, and methicillin resistant *S. aureus* (MRSA) clinical isolates exhibiting the MIC and MBC values of 2200, 2400 µg/ml and 2300, 2700 µg/ml, respectively. Substantial inhibitory effects of ALE-ZnONPs on bacterial growth kinetics, exopolysaccharides and biofilm formation, unequivocally suggested the antibiotic and anti-biofilm potential. Overall, the results elucidated a rapid, environmentally benign, cost-effective, and convenient method for ALE-ZnONPs synthesis, for possible applications as nanoantibiotics or drug carriers.

Key words: *Aloe vera*, ZnO nanoparticles, biogenic synthesis, biofilm inhibition

1. Introduction

A rapid stride in synthesis and applications of nanomaterials, in recent years, has been perceived in almost every domain of life including health care, cosmetics, biomedical, food and feed, drug-gene delivery, environment, electronics, mechanics, catalysis, energy science, optics, chemical and space industries [1]. Nanoparticles (NPs) of noble metals, such as gold, silver, platinum, and zinc oxide are widely used in medical and pharmaceutical applications, and in an array of consumer products [2]. Synthesis of NPs has been reported using various chemical and physical methods, such as sol-gel process, chemical precipitation, chemical vapour deposition, hydrothermal and microwave methods [3]. Lately, single-pot biomimetic and/or biological methods of synthesis are preferred over chemical and physical methods because of their rapidity, eco-friendliness, non-pathogenic, and economical attributes. Besides, these methods exclude the use of high temperature, pressure, energy and toxic chemicals [4]. Furthermore, the metallic NPs are recently being comprehended as promising nanoantibiotics, due to their remarkable antimicrobial properties. This has elicited enormous research interest owing to growing incidence of multiple antibiotic resistance in microorganisms [5]. Lately, environmentally friendly single-step protocols using plants extracts without involving any extrinsic surfactants, capping agents, and/or templates have been explored for metal NPs synthesis [6]. This intrinsically green approach involves the biomolecules such as proteins, amino acids, enzymes, vitamins, alkaloids, phenolics, saponins, tannins, and terpinoids, present in plant extracts, for reduction and stabilization of metal ions [7]. Some of these biomolecules act as electron shuttles in metal reduction, while other constituents are responsible for capping of resulting NPs, which not only controls the aggregation of NPs but also results in post-surface modification of NPs [8].

This has prompted us to use *Aloe barbadensis Miller (A. vera) plant* extract for synthesis of zinc oxide nanoparticles (ZnONPs). Zinc oxide has been chosen because of its wide spectrum applications in sunscreens, paints, plastic and rubber manufacturing, pharmaceutical products, diagnostics and micro-electronics [9]. The ZnONPs have also been used to remove arsenic and sulphur from water [10], and in dental applications [11]. They have also been shown to exhibit strong protein adsorption properties, which can be used to modulate cytotoxicity, metabolism and other cellular responses [12]. Also, due to its low toxicity, ZnO has been listed as "Generally Recognized as Safe" (GRAS) by the US Food and Drug Administration (21, CFR 182, 8991). Therefore, *A. vera* extract has been used to synthesize (ALE)-capped ZnONPs, by reduction of $ZnSO_4$ without involving any supplementary chemicals or physical steps. *A. vera* is a perennial plant of the Liliaceae family. It is an important natural medicinal plant [13-15] with anti-inflammatory [16], anti-arthritic activity [17], and antibacterial effects [18]. The extract of this plant has been used for synthesis of gold NPs (~50-350 nm), silver NPs (~15 nm) [19]

and zinc oxide NPs (35 nm) [20]. Earlier studies with *A. vera* plant extract have reported the synthesis of ZnONPs (27 nm), but at 100^0C, pH 6.0 [21], and also 35 nm particles with 25% *Aloe* gel extract at a much higher temperature of 150^oC, under alkaline conditions [20]. On the contrary, this study demonstrates the synthesis of smaller size ZnONPs at 60^0C, pH 8.0, based on the experiments performed as a function of ALE concentration and pH of reaction medium, in order to achieve optimal nucleation. Besides, the stability and internalization of ALE-ZnONPs have been assessed and their antibacterial and anti-biofilm potential determined, based on bacterial growth inhibition, exopolysaccharides production, minimum inhibitory concentration (MIC) and minimum bactericidal concentration (MBC), against the extended spectrum β-lactamase (ESBL) producing *Pseudomonas aeruginosa, Escherichia coli* and Gram-positive methicillin-resistant *Staphylococcus aureus* (MRSA) and methicillin-sensitive *Staphylococcus aureus* (MSSA) clinical isolates.

2.0. Materials and methods

2.1. Bacterial strains and culture conditions

The bacterial cultures of *E. coli* (ATCC 25922), *P. aeuruginosa* (ATCC 27853) and *S. aureus* (ATCC 95923) and the clinical bacterial isolates, such as extended spectrum β-lactamase (ESBL) producing *E. coli-336, P. aeruginosa-621,* Methicillin-resistant *S. aureus* MR-1 (MRSA) and Methicillin-sensitive *S. aureus (MSSA-6),* were obtained from the Department of Microbiology, Jawaharlal Nehru Medical College, AMU, Aligarh, India. The standard strains and isolates were sub-cultured in Luria broth (LB), Mueller-Hinton (MH) and Brain heart infusion (BHI) broths. The cultures were stored at -20 ^{0}C in 20% glycerol, for long term preservation. All experiments were performed with the freshly grown cultures.

2.2. Preparation of the Aloe vera leaf extract (ALE)

Aloe vera leaves were collected from plants growing in garden of the Faculty of Agricultural Sciences, Aligarh Muslim University, Aligarh (latitude and longitude coordinates: 27.913 and 78.078), India. Leaves were washed thoroughly with distilled water to remove all dust particles. Extract was prepared by blending 20g of finely chopped skin of leaves in 100 ml of autoclaved deionized Milli Q water in a 250 ml glass conical flask. The mixture was kept for 10 min in a water bath at 60^0C. Colour of the aqueous solution changed from watery to light green. The extract was cooled at room temperature, filtered through Whatman filter paper No.1 and stored at 4^0C for further use.

2.3. Synthesis of ALE capped ZnONPs

For synthesis of ALE-ZnONPs, the stock ALE (40 ml) was added to obtain an ALE:$ZnSO_4$ ratio of 1:4 (v/v), maintaining final $ZnSO_4$ concentration of 0.25M. The reaction mixture (200 ml) was stirred vigorously for 3 h at 60^0C, and centrifuged at 4500 rpm for 10 min. The cream coloured pellet was washed with Milli Q water, dried at 80^0C in vacuum oven for 24 h. For optimum synthesis of ALE-ZnONPs, the separate sets of experiments were performed as a function of ALE concentration and pH of reaction medium. Briefly, varying concentrations of ALE (10, 20, 30, 40 and 50%) were added to 100 ml of 0.25 M $ZnSO_4$ solution in different glass flasks. Similarly, in another set of experiments, the pH of the reaction mixture, in the range of pH 5.0-10.0, was achieved by adding 0.1 M HCl and NaOH. In each case, the reaction mixture was kept under vigorous stirring at 60^0C for 3 h. The precipitate obtained was centrifuged at 4500 rpm for 10 min, thoroughly washed and dried at 80^0C for 24 h. The resultant dried material was powdered and stored in an airtight container for further analysis.

2.4. Characterization of ALE-ZnONPs.

2.4.1. UV-visible and fluorescence spectral analyses

The biosynthesized colloidal ALE-ZnONPs were analysed for surface plasmon resonance (SPR) by use of a double beam UV-Vis spectrophotometer (UV5704S from Electronics, India Ltd) in the wave length range of 200 - 700 nm.

2.4.2. X-ray diffraction measurements

The X-ray diffraction (XRD) pattern of powdered ALE-ZnONPs was recorded on MiniFlex™ II XRD system (Rigaku Corporation, Tokyo, Japan) at 40 kV with CuKα radiation (k = 1.54 Å). The crystalline size of the ALE-ZnONPs was calculated following the Debye–Scherrer's formula: $D = 0.9\lambda/\beta\cos\theta$: whereas, D is the crystal size of ALE-ZnONPs, λ is the wavelength of X-ray source used (1.541^{O}A), β is the full-width-at-half-maximum of the diffraction peak [22].

2.4.3. Scanning electron microscopy (SEM) and ALE-ZnONPs bacterial interactions

SEM analysis was carried out using fine powder of ALE-ZnONPs by use of JSM 6510LV scanning electron microscope (JEOL, Tokyo, Japan) at an accelerating voltage of 15 kV. The elemental analysis of ALE-ZnONPs was performed using Oxford Instruments INCAx-sight EDAX spectrometer equipped SEM.

2.4.4. Transmission electron microscopy (TEM)

TEM was performed on JEOL 100/120 kV TEM (JEOL, Tokyo, Japan) at an accelerating voltage of 200 kV. Samples for microscopy were prepared by dropping 10µl of ALE-ZnONPs sample on a copper grid. The copper grid was then dried for 6 h in an oven at 80^0C.

2.4.5. Fourier transform infrared (FTIR) spectroscopy and GC-MS analysis

FTIR was employed for assessment of functional groups on ALE and ALE-ZnONPs. Briefly, the air dried powder of ALE and ALE-ZnONPs were mixed separately with spectroscopic grade KBr (1:100) and the spectra recorded. FTIR measurements were carried out by use of Perkin Elmer FTIR spectrometer, Spectrum Two (CT, USA) in diffuse reflectance mode, at a resolution of 4 cm^{-1} in KBr pellets. GC-MS analysis of ALE was performed by use of SHIMAZDU QP2010, Column Rtx-5 MS (30 meter X 0.25 mm i.d.X 0.25 um film thickness),oven temperature 50˚C to 280˚C at 4˚C/min, for 5 min; inlet and interface temperatures were 250˚C and 280˚C, respectively. Carrier gas was He at a flow rate of 1.0 ml/min (constant flow). 0.2 ml of sample was injected under split of 20:1. EIMS: electron energy, 70 eV. Interpretation of mass spectrum GC-MS was conducted using data base of NIST, having more than 62,000 patterns. The spectrum of the known compounds was compared with the NIST library.

2.5. Evaluation of antibacterial activity of ALE-ZnONPs

2.5.1. Determination of MIC and MBC of ALE-ZnONPs

The MIC and MBC values of ALE-ZnONPs against the *E. coli, P. aeruginosa* (ESBL), MRSA, and MSSA isolates were determined following the procedure described by Ansari et al. [23]

2.5.2. Time-dependent growth inhibition assay

The effect of ALE-ZnONPs on the growth of *E. coli, P. aeruginosa* (ESBL), MRSA, and MSSA isolates was assessed by optical density measurements [24-25]. Aliquots of 100 µl each of exponentially grown bacterial cultures were transferred to sterile 2 ml LB in test tubes containing ALE-ZnONPs at an increasing concentration range of 250-2000 µg/ml, under aseptic conditions. Subsequently, 100 µl of untreated and treated samples from each tube were transferred to the wells in a microtitre plate and incubated for 16 h at 37^0C. The absorbance was measured at 620 nm at a regular interval of 4 h by use of a microplate reader (Thermo Scientific Multiskan EX, REF 51118170, China).

2.5.3. Effect of ALE-ZnONPs on biofilm formation

To determine the effect ALE-ZnONPs on biofilm formation by *E.coli, P. aeruginosa* and *S. aureus*, the microtitre plate assay was performed following the method of Dwivedi et al. [26]. Briefly, the wells of sterile polystyrene microtitre plate were seeded with 100 µl of freshly grown bacterial cells (1 x 10^7 CFU/ml) in LB. To each well, ALE-ZnONPs were added in an increasing concentration range of 250-2000 µg/ml. The plates were incubated in a static condition at 37^0C for 24 h. Controls wells were maintained with medium containing bacterial suspension without ALE-ZnONPs. The suspension was then removed and the wells were washed with sterile 1X PBS, to remove loosely attached bacteria. Wells were then stained with 200 µl of 0.25% crystal violet and incubated for 30 min. The wells were washed, air dried, and bound stain was solubilized in 200 µl of 95% ethanol. The absorbance was read at 620 nm by use of a microplate reader (Thermo scientific Multiskan EX, REF 51118170, China).

2.5.4. Microscopic analysis of bacterial biofilm formation.

The biofilm inhibition was studied under an optical microscope (Olympus BX60, Model BX60F5, Olympus Optical Co. Ltd. Japan) equipped with colour VGA camera (Sony, Model no. SSC-DC-58AP, Japan). Briefly, 1% of overnight grown cultures of the *E. coli, P. aeruginosa* (ESBL) and *S. aureus* (MRSA & MSSA) were transferred to 2 ml of fresh LB medium without and with ALE-ZnONPs in concentration range of 250-2000 µg/ml, in 6-well polystyrene plate carrying cover slip of 1 x 1 cm. The plates were then incubated for 24 h at 37 ^{0}C. The biofilms adhered on to the cover glasses were stained with 0.1% crystal violet (Hi-Media, Mumbai, India) and visualised at 100 X magnification.[27].

2.5.5. Effect of ALE-ZnONPs on extracellular polysaccharides (EPS) production.

The EPS production by the bacteria grown in the absence and presence of ALE-ZnONPs (0-500µg/ml) at 37^0C for 24 h was determined following the method of Khan et al. [28]. In brief, ALE-ZnONPs treated and untreated bacterial cells were harvested by centrifugation at 10,000 rpm for 15 min. The cell pellets were resuspended in 5 ml PBS (pH 7.0) and centrifuged at 10,000 rpm for 30 min. The supernatant was collected in fresh tube and the dissolved EPS was precipitated from the supernatant by adding three volumes of 95% ethanol. EPS precipitate was resuspended in 500µl of Milli-Q water. For quantification, 200 µl of EPS solution was mixed with equal volume of ice cold 5% phenol and 1 ml of concentrated H_2SO_4. The intensity of red colour developed was measured spectrophotometrically at 490 nm.

2.5.6. Assessment of NPs internalization by flow cytometry (FCM) and atomic absorption spectrophotometry (AAS).

Freshly grown suspensions of *E. coli* and *S. aureus* cells (~10^9 CFU/ml) were treated at increasing concentrations (25-100 µg/ml) of ALE-ZnONPs for 12 h at 37^0C, on a shaking incubator at 180 rpm. Surface adsorption and uptake of ALE-ZnONPs in bacterial cells were assessed by use of a flow cytometer (FACS Caliber, BD Biosciences, San Jose, CA, USA) following the method of Kumar et al. [29]. Briefly, 50 µl of treated cells were added to 950 µl of 1X PBS, mixed thoroughly and analysed using Cell Quest Pro software (BD Biosciences). The forward scatter (FSC) and side scatter (SSC) intensities, indicating the size and intracellular density of cells, respectively, were recorded. Gating of the data as P1 and P2 was based on SSC and FSC of control cells. It helps to differentiate the cells in which internalization of NPs has occurred (P1) with those where only adsorption or both internalization and adsorption have occurred (P2). Gating in dot plots was kept identical throughout and without any compensation. Furthermore, the intracellular Zn in bacterial cells was quantified by use of AAS. In brief, 10 ml of freshly grown bacterial cells were treated with ALE-ZnONPs (1000 µg/ml) at 37^0C for 24 h. The cells were centrifuged at 3000 rpm for 15 min. Both the pellet and cell-free supernatant were collected separately. The wet cell pellet was digested with 5ml of aqua regia (HNO_3 : HCl, 1:3 v/v) at 60^0C for 30 min. The volume was then adjusted to 100 ml with distilled water in a volumetric flask for analysis by use of a double beam atomic absorption spectrophotometer (GBC Model 932B plus, Australia).

2.5.7. Intracellular ROS production by ALE-ZnONPs

Intracellular ROS produced by ALE-ZnONPs in bacterial cells were measured with an oxidation-sensitive fluorescent probe 2,7-dichlorofluorescein diacetate (DCFH-DA) [26]. The DCFH-DA passively diffuses through the cell membrane into the cell and is deacetylated by esterases to form non-fluorescent 2,7-dichlorofluor-escein(DCFH). The DCFH reacts with ROS to form the fluorescent product 2,7-dichlorofluorescein (DCF) [24], which is trapped inside the cell making fluorescent. In brief, the freshly cultured bacteria (10^8 cfu/mL) were washed three times with fresh medium. DCFH-DA was mixed with the cultures at a ratio of 1:2000 and the mixture was shaken for 30 min at 37^{o}C. The cells were then pelleted by centrifugation and washed two times to remove the DCFH. Cells were exposed to ALE-ZnO-NPs at increasing concentrations in the range of 250–2000 µg/mL. Fluorescence intensity of DCF was measured by use of fluorescence spectrophotometer at an excitation wavelength of 488 nm and at an emission wavelength of 535 nm. Furthermore, the treated and control cells were visualized under a fluorescence microscope (Olympus BX60, Model BX60F5, Olympus Optical Co. Ltd. Japan) equipped with colour VGA camera (Sony, Model no. SSC-DC-58AP, Japan) for validation of ALE-ZnONPs induced ROS generation.

2.6. Statistical analyses

Data were expressed as mean ± S.D. for the values obtained from at least two independent experiments done in triplicate. Statistical analysis was performed by one-way analysis of variance (ANOVA) using Holm-Sidak method, multiple comparisons versus control group (Sigma Plot 11.0, USA). The level of statistical significance chosen was *$p < 0.05$, unless otherwise stated.

3.0. Results and Discussion

3.1. Biosynthesis of ALE-ZnONPs

The reducing potential of ALE has been exploited for biosynthesis of ZnONPs. Fig. 1A shows the UV-vis spectra of ALE, $ZnSO_4$ and ALE-ZnONPs, in an aqueous suspension. A characteristic peak of ALE-ZnONPs was recorded at 375 nm, whereas no absorption peaks of ALE or $ZnSO_4$ were observed. Indeed, zinc oxide is known to exhibit absorption in the range of 300–500 nm, and a characteristic peak of ZnONPs at 372 nm has been demonstrated by Nagarajan and Kuppusamy [30]. Also, Sangeetha et al. [20] have reported the absorption peak of ZnONPs in the range of 358-375, due to surface plasmon

resonance. Addition of leaf extract in increasing amounts to aqueous $ZnSO_4$ solution, resulted the change in colour from off white to yellowish brown to reddish brown, and finally to colloidal brown, indicating ZnONPs formation. Similar changes in colour have also been reported in previous studies [31-35]. The ALE-ZnONPs were quite stable as no significant change in the absorbance of the colloidal ALE-ZnONPs solution occurred up to six months (Fig.1B). Results in Fig. 1 C and D show a blue shift with increasing ALE concentration in the range of 10 % to 50 %, and in the pH range of 5.0 to 10.0. The UV-vis spectra indicated optimum bioreduction with 10% leaf extract as a reducing agent at pH 8.0, under our experimental conditions (Fig.1C and D). Nagarajan and Kuppusamy [30] have reported similar observations with increasing concentrations of sea weed *Sargassum myriocystum* mediated synthesis of ZnONPs. At a lower pH range of 5.0 to 7.0, much lesser absorption was noticed. This could be plausibly due to aggregation rather than nucleation of ZnONPs to form larger particles. Whereas, a sharp peak at pH 8.0 indicated maximum reduction of zinc sulphate to ZnONPs. It has been speculated that benzoquinones in plant extracts might act as reducing agents during formation of NPs [36]. Besides, the enzymes and proteins in extract are also known to control the size and shape of the NPs by weaker binding with nascent ZnO nanocrystals, which lead to isotropic growth of the crystals, and formation of ZnONPs. [37]. Thus, in comparison to *Aloe* gel broth, which reportedly took a longer nucleation time (5-6 h) at an elevated temperature of 150^0C [20], the ZnONPs synthesis of 8 - 20 nm in this study with *Aloe* skin extract, within 3 h, at a much lower temperature of 60^0C, could be a better alternative.

3.2. X-Ray diffraction analysis

Fig. 2A shows distinctive Bragg reflections at 2θ values of 31.84^0, 34.45^0, 36.30^0, 47.59^0, 47.59^0, 47.59^0, 56.70^0, 62.88^0, 66.50^0, 68.04^0, 69.21^0, 72.55^0 and 77.07^0 can be indexed to the (100), (002), (101), (102), (110), (103), (200), (112) and (201) that are in good agreement with wurtzite ZnO (JCPDS CARD NO: 36- 1451). The distinct and clear peaks confirmed the high purity and crystalline nature of the prepared ALE-ZnONPs. The full-width-at-half-maximum (FWHM) value for (101) plane of reflection was used to calculate the size of the NPs, and the average particle size of the ALE-ZnONPs has been determined to be 15 nm, under our experimental conditions.

3.3. FTIR and GC-MS analyses

The FTIR spectra of *A. vera* leaf extract alone and ALE-ZnONPs are shown in Fig. 2B. The spectra exhibited a broad peak at 3432 cm^{-1}, assigned to the -OH group from phenol present in the extract. The bands at 3452 and 2934 cm^{-1} are attributed to stretching vibrations of the amines, O-H stretching of alcohols and C-H stretching of alkanes. Similar band pattern has been reported by Sangeetha *et al.* [20] for the ZnONPs synthesized by *A. barbadensis* miller leaf extract. The peak at 1634 cm^{-1} is due to the amide regions that are characteristics of proteins and enzymes. The high intensity band around 440 cm^{-1} is due to stretching mode of zinc and oxygen bond [38-40]. Thus, our result concurs with the observations of Sangeetha et al. [20], indicating the role of phenolic compounds, terpenoids and proteins in synthesis and stability of ZnONPs. Proteins are known to form a corona around NPs, making them more dispersible and prevent agglomeration in aqueous medium. Furthermore, the free amino and carboxylic groups interaction with zinc surface, reportedly contributes for stability of ZnONPs [20]. The chromatogram of GC-MS shows that the active ingredients in ALE (Fig.3). The results recorded approximately 38 active compounds within 48 min. of retention time (Table 1). The data analysis revealed the presence of at least four major compounds based on prominent peaks in chromatogram (at peak number 4, 9, 13 and 36) namely as ethanone, 1-phenyl (C_8H_8O), guanosine ($C_{10}H_{13}N_5O_5$), pentadecanoic acid ($C_{15}H_{30}O_2$) and tetraconate ($C_{40}H_{82)}$ with maximum peak areas determined to be 13.15%, 19.35%, 6.86% and 29.84 %, respectively. Therefore, ethanone, 1-phenyl, guanosine, pentadecanoic acid and tetraconate could be the likely candidates involved in capping ZnO at nano scale besides proteins and other auxiliary phytochemicals, which needs to be ascertained in further studies.

3.4. SEM, TEM and EDX analyses

The SEM images at 10,000 X magnification exhibited pleomorphic ALE-capped ZnONPs (Fig.4A). The elemental composition of ZnONPs was analysed through EDX, and found comprised of zinc (63.12%) and oxygen (36.88%) (Fig.4B). Results indicate three emission peaks of metallic zinc and asmall peaks of oxygen, which confirmed the formation of ALE-ZnONPs. Furthermore, the TEM image exhibited ALE-ZnONPs of different shapes as spherical, oval and hexagonal in size range of 8-18nm (Fig.4C and D). Based on size frequency analysis, a majority of ALE-ZnONPs were found to be of size 14 nm, which corresponds well with the XRD data.

3.5. Antibacterial and anti-biofilm activity of ALE-ZnONPs

The ALE-ZnONPs were evaluated for their antimicrobial activity against ESBL producing and methicillin sensitive and resistant bacteria. The results shown in Fig.5 A-F demonstrate a differential growth inhibition pattern of ESBL producing *E. coli*, *P. aeruginosa* and methicillin resistant *S. aureus-1*, *E. coli* (ATCC 25922), *P. aeuruginosa* (ATCC 27853) and *S. aureus* (ATCC 95923) at increasing concentrations of ALE-ZnONPs. The Gram -ve (*E. coli and P. aeuruginosa*) cells were found to be more sensitive and susceptible to ALE-ZnONPs than Gram +ve bacteria (*S. aureus*). Within the category of Gram +ve cells, the MSSA (ATCC 95923) was found to be more sensitive (21.75±.02% survival) to ALE-ZnONPs, compared with MRSA-1 (28.91±.0.1 % survival). While, amongst the ESBL producers, the *E. coli* cells were the most sensitive (29% survival). The MIC and MBC values of ALE-ZnONPs for the ESBL producing *E. coli* and *P. aeruginosa* were determined to be 2200 and 2400 µg/ml and 2300 and 2700µg/ml, respectively. Whereas, the MIC and MBC values of ALE-ZnONPs with MRSA and MSSA were estimated to be 2000 and 2200 µg/ml, and 2200 and 2400 µg/ml, under identical conditions (Table 2). Fig.6A-D shows the effect of ALE-ZnONPs on *E. coli* and *S. aureus* cells at a sub-lethal concentrations of 1000 µg/ml. The representative SEM images revealed substantial ALE-ZnONPs induced cellular damage in treated cells compared with untreated control.

Fig.7 A (I-III) shows the representative micrographs indicating ALE-ZnONPs concentration dependent inhibition of biofilm formation by the *E. coli, P. aeruginosa* and *S. aureus* cells. The data revealed 22.1 ± 5.0, 21.9 ± 3.0 and 18.8 ± 3.0 % inhibition of biofilm formation in *E. coli* ESBL-336; 60.5 ± 5.0, 53.9 ± 3.0 and 41.5 ± 3.0 % in *P. aeruginosa-621*; whereas 55.3 ± 3.0, 28.3 ± 3.0 and 20.4 ± 3.0 % in MRSA-1, as compared to control (Fig. 7B). Both the *E. coli* (ATCC 25922) and *P. aeruginosa*-621 are also known to be potent biofilm producers, which makes their clinical management difficult. Successful treatment becomes more challenging with increasing prevalence of ESBL producing bacteria and antibiotic inefficacy, particularly when such bacteria are involved in chronic infections. Thus, ALE-ZnONPs induced quorum quenching could be an alternate strategy for combating biofilm based bacterial infections. Nevertheless, it could be argued that the phytochemicals, such as vitamins, enzymes, minerals, sugars, salicyclic acids, lignins, saponins, amino acids acid and anthraquinones present in plant leaf extracts may act like a strong siderophores, which chelate iron from the medium and results in degradation of bacterial biofilm [41]. Indeed, *A. vera* leaves are reported to contain as many as 75 nutrients and 200 active compounds of the major components of anthraquinones (aloin, anthranol and aloetic acid) with vitamins (B1, B2, B6, choline folic, acid ascorbic, β carotene, etc.), as minor substances [42-43]. However, under our experimental conditions, the heat treatment of ALE at 80^0C, most likely resulted in thermal degradation of such phytocompounds. Therefore, no bacterial

growth activity with ALE alone, or with bulk material ($ZnSO_4$) was observed, which explicitly suggests the role of ALE-ZnONPs in significant inhibition of biofilm formation.

The ALE-ZnONPs induced reduction in EPS production by ESBL producing *E. coli* and *P. aeruginosa*, and MRSA is shown in Fig.8. The ESBL producing Gram -ve bacteria *E. coli*, and *P. aeruginosa* exhibited 19.68 to 83.28% ($p<0.05$) and 15.23% to 66.43% ($p<0.05$) inhibition of EPS in presence of ALE-ZnONPs, respectively, whereas, Gram +ve MRSA showed 22.72% to 87.36% ($p<0.05$) inhibition in EPS production at concentration range of 50 to 500µg/ml. The results suggested ALE-ZnONPs induced EPS inhibition in the order as *S. aureus* > (MRSA).*E. coli* (ESBL) > *P. aeruginosa* (ESBL)

3.6. Flow cytometry and AAS analysis of ALE-ZnONPs uptake in bacteria

Fig.9A-B shows the flow cytometry data related to surface interaction and internalization of ALE-ZnONPs in *E. coli* and *MRSA* cells. Significant increase in intensity of side scatter (SSC) compared to control suggested the uptake of ALE-ZnONPs both in the Gram -ve *E. coli* and Gram +ve *S. aureus* cells, in a concentration dependent manner upon treatment with increasing concentrations of ALE-ZnONPs (25-100 µg/ml). Gated population (P2) show percentage of cells with increased granularity without any increase in the size, as an indicator of internalization. The data suggested 3.6, 6.6, 9.7-fold increase in granularity in *E. coli* cells treated with 25, 50, and 100 µg/ml ALE-ZnONPs, respectively. Similarly, MRSA cells also exhibited uptake of ALE-ZnONPs, and have indicated an increase in the granularity by 1.0, 1.7, 1.9-fold, under identical conditions. Besides, the treated MRSA cells also exhibited a minor change in size, as evident by increase in FSC values (P1). The presence of intracellular ALE-ZnONPs has been further validated by quantitative AAS analysis, which revealed intracellular concentration of 58.61% and 3.15% Zn^{2+} in Gram -ve *E. coli* and Gram +ve *S. aureus* cells, respectively (Table 3). It is expected that the high solubility of ZnO nanopowder in the bacterial culture media suggested the formation of aqueous complexes of zinc ions with organic or inorganic constituents of the complex media. The release of Zn^{2+} ions from ZnO by the medium, may causes transportation of Zn^{2+} ions into the interior cell wall resulting in bacteriostatic effect. Such interactions between the cell envelope components and Zn^{2+} ions from ZnO have also be suggested by Zhang et al. [44], which supports our observations.

3.7. Enhanced ROS production in presence of ALE -ZnONPs-bacteria interface.

ROS production upon addition of ALE-ZnONPs has been evaluated using the fluorescence dye, DCFH-DA, as a ROS indicator [45]. Fig 10A-C indicates some residual ROS generation in absence of ALE-ZnONPs, i.e. in control culture, since the dye exhibits anincrease in quantum yield with bacterial

growth. The ROS produced under non-stress conditions are counter balanced by ROS scavenging enzymes present in bacteria. However, in presence of 250-2000µg/mL of ALE-ZnONPs, ROS production was much greater and determined to be 102 ± 4–358 ± 8%, 118 ± 8-256 ± 6% and 100.8 ± 6-137 ± 6 in *E. coli*, *P. aeruginosa* and *S. aureus* respectively. This has resulted in significant decline in population of viable bacterial cells Fig.11. Additionally, *E. coli* and *P. aeruginosa* cultures show higher ROS production on ALE-ZnONPs treatment in comparison to *S. aureus* culture, which can be rationalised with the difference in magnitude of change in interfacial potential for both the Gram -ve and Gram +ve categories of bacteria. The surface potential neutralization of bacteria has been reported to trigger the production of ROS, which is considered responsible for lipid, protein and DNA damage, resulting into non-viable bacterial population [46-47].

4.0. Conclusion

In conclusion, our result validated the development of a rapid and eco-friendly single-pot biological method of ZnONPs synthesis exploiting the reducing and capping potential of *Aloe barbadensis* Miller (*A. vera*) leaf extract (ALE). This is the third report on biogenic synthesis of highly crystalline ALE-capped ZnONPs (8 to 20 nm) within 3 h, at relatively lower temperature of 60^0C and pH 8.0, compared with the existing methods, which take a longer nucleation time of 5-6 h at an elevated temperature of 150^0C under alkaline [20] or 100^0C under acidic [21] reaction conditions. This method is a better alternative, which precludes the use of high temperature, pressure, energy and toxic chemicals in metal NPs synthesis without requiring any extrinsic surfactants or capping agents. The distinct and clear XRD peaks suggested the high purity and crystalline nature of ALE-ZnONPs. The elemental composition of ZnONPs as zinc (63.12%) and oxygen (36.88%) obtained through SEM-EDX, confirmed the formation of ALE-ZnONPs. GC-MS analysis of ALE-ZnONPs revealed the predominance of compounds like ethanone, 1-phenyl, guanosine, pentadecanoic acid and tetraconate in ALE, which might be responsible for conferring stability to associated ZnONPs, besides proteins and other auxiliary phytochemicals. The ALE phytochemicals specificity as presumptive stabilizers and capping agents is speculative and needs to be ascertained in future studies. Flow cytometry data on surface interaction and internalization of ALE-ZnONPs in bacteria suggested the uptake of ALE-ZnONPs both in the Gram -ve *E. coli* and Gram +ve *S. aureus* cells, in a concentration dependent manner. ALE-ZnONPs exhibited differential antibacterial activity against the Gram -ve and Gram +ve bacterial cells. The results also demonstrated ALE-ZnONPs induced EPS inhibition in the order as *E. coli* (ESBL) > *P. aeruginosa* (ESBL) >*S. aureus* (MRSA). Greater sensitivity of *E. coli* cells to ALE-ZnONPs is most likely due to stronger cell proliferation and interaction with cellular components vis-à-vis Gram +ve *S. aureus* cells. The NPs with strong antimicrobial and anti-biofilm activities are envisaged as prospective nanoantibiotics, effective

against the bacterial strains resilient to conventional antibiotics. Nevertheless, the area specific, varietal and seasonal variations in chemical constituents of plant extracts may often lead to different results in different laboratories, which warrant further studies in identification of key plant biomolecules or metabolites for developing more efficient technology for NPs synthesis.

Conflict of interest

There is no conflict of interest.

Acknowledgments

This project was financially supported by King Saud University, Vice Deanship of Research Chairs"

References:

[1] S. Tachikawa, A. Noguchi, T. Tsuge, M. Hara, O. Odawara, H. Wada, Optical Properties of ZnO Nanoparticles Capped with Polymers, Materials 4 (2011) 1132-1143.

[2] A. N. Sahu, Nanotechnology in herbal medicines and cosmetics, Int. Res. Ayurveda Pharma. 4 (2013) 3.

[3] P. Logeswari, S. Silambarasan, J. Abraham, Eco friendly synthesis of silver nanoparticles from commercially available plant powders and their antibacterial properties, Scientia. Iranica. Transactions F: Nanotechnol. 20 (2013) 1049–1054.

[4] D. Gnanasangeetha, S. Thambavani, One Pot Synthesis of Zinc Oxide Nanoparticles via Chemical and Green Method, Res. J. Material Sci. 1 (7) (2013) 1-8.

[5] J. Lakshmi V, R. Sharath, M.N. Chandraprabha, E. Neelufar, A. Hazra, M. Patra, Synthesis, characterization and evaluation of antimicrobial activity of zinc oxide nanoparticles, J. Biochem. Tech. 3 (2012) 151-154.

[6] Y. Zhang, D.Yang, Y. Kong, X. Wang, O. Pandoli, G. Gao, Synergetic Antibacterial Effects of Silver Nanoparticles *Aloe Vera* Prepared via a Green Method, Nano. Biomed. Eng. 2 (2010) 252-257.

[7] A.K. Jha, K. Orasad, K. Prasad, A.R. Kulakarni, Plant system: natures nanofactory, Colloids Surf. B: Biointerfaces 73 (2009) 219-223.

[8] F. Okafor, A. Janen, T. Kukhtareva, V. Edwards, M. Curley, Green Synthesis of Silver Nanoparticles, Their Characterization, Application and Antibacterial Activity, Int. J. Environ. Res. Public Health 10 (2013) 5221-5238.

[10] K. Dhermendre, Tiwari, J. Behari, P. Sen, Application of nanoparticles in waste water treatment, World Appl. Sci. J. 3 (2008) 417-433.

[11] M.M. Tomczak, M.K. Gupta, L.F. Drummy, S.M. Rozenbak, R.R. Naik, Morphological control and assembly of Zinc oxide using biotemplat, Acta Biomater. 5 (2009) 876–882.

[12] M. Horie, Nishiok, K. Fujit, Protein adsorption of ultra fine metal oxide and its influence on cytotoxicity toward cultural cell, Chem. Res. Toxicol. 22 (2009) 543-53.

[13] O.O. Agarry, M.T. Olaleye, B. Michael, C.O, Comparative antimicrobial activities of *Aloe vera* gel and leaf, Afr. J. Biotechnol. 4 (2005) 1413-1414.

[14] J. Barnes, L. A. Anderson, J.D. Phillipson, A guide for health-care for health-care professionals, Herbal Medicines (1996) 296.

[15] R.H. Davis, J.J. Donato, G.M. Hartman, R.C. Haa, Anti-inflammatory and wound healing activity of a growth substance in *Aloe vera*, J. Am. Podiatr. Med. Assoc. 84 (1994) 77-81.

[16] B. Vázquez, G. Avila, D. Segura, B. Escalante, Anti-inflammatory activity of extracts from *Aloe vera* gel, J. Ethnopharmacol 55 (1996) 69-75.

[17] Q. Feng, J. Wu, G. Chen, F. Cui, T. Kim, J. Kim, A mechanistic study of the antibacterial effect of silver ions on *Escherichia coli* and *Staphylococcus aureus*, J. Biomed. Mater. Res. Part A 52 (2000) 662-668.

[18] S. Chandran, M. Chaudhary, R. Pasricha, A. Ahmad, M. Sastry, Synthesis of gold nanotriangles and silver nanoparticles using *Aloe vera* plant extract, Biotechnol. Prog. 22 (2006) 577-583.

[19] J.L. Venkataraju, R. Sharath, M.N. Chandraprabha, E. Neelufar, A. Hazra, M. Patra, Synthesis, characterization and evaluation of antimicrobial activity of zinc oxide nanoparticles, J. Biochem. Tech. 3 (2012) S151-S154.

[20] G. Sangeetha, S. Rajeshwari, R. Venckatesh, Green synthesis of zinc oxide nanoparticles by *aloe barbadensis miller* leaf extract:Structure and optical properties. Mater. Res. Bull. 46 (2011) 2560–2566.

[21] A. Ayeshamariam, M. Kashif, V.S. Vidhya, M.G.V. Sankaracharyulu, V. Swaminathan, M. Bououdina, M. Jayachandran, Biosynthesis of (Zno–aloe vera) nanocomposites and antibacterial/antifungal studies, J. Optoelect. Biomed. Mater. 6 (2014) 85- 99.

[22] A.L. Patterson, The Scherrer Formula for X-Ray Particle Size Determination, Phys. Rev. 56 (1939) 978.

[23] M.A. Ansari, H.M. Khan, M.A. Alzohairy, M. Jalal, S.G. Ali, R. Pal, J. Musarrat, Green synthesis of Al2O3 nanoparticles and their bactericidal potential against clinical isolates of multi-drug resistant Pseudomonas aeruginosa. World J Microbiol Biotechnol 31(2015) 153-64.

[24] K. Ali, B. Ahmed, S. Dwivedi, Q. Saquib, A.A. Al-Khedhairy, J.Musarrat, Microwave Accelerated Green Synthesis of Stable Silver Nanoparticles with Eucalyptus globulus Leaf Extract and Their Antibacterial and Antibiofilm Activity on Clinical Isolates. PLoS One 10 (2015) e0131178.

[25] R. Wahab, S.T. Khan, S. Dwivedi, M. Ahamed, J. Musarrat, AA Al-Khedhairy, Effective inhibition of bacterial respiration and growth by CuO microspheres composed of thin nanosheets. Colloids Surf. B: Biointerfaces 111(2013) 211-217

[26] S. Dwivedi, R. Wahab, F. Khan, Y.K. Mishra, J. Musarrat, Reactive Oxygen Species Mediated Bacterial Biofilm Inhibition via Zinc Oxide Nanoparticles and Their Statistical Determination. PLoS ONE 9 (2014) 111289.

[27] S. T. Khan, M. Ahamed, A.A. Al-Khedhairy, J. Musarrat, Biocidal effect of copper and zinc oxide nanoparticles on human oral microbiome and biofilm formation, Mat. Lett. 97 (2013) 67–70

[28] S.T. Khan, M. Ahmed, H.A. Alhadlaq, J. Musarrat, A.A. Khaidhairy, Comparative effectiveness of $NiCl_2$, Ni- and NiO-NPs in controlling oral bacterial growth and biofilm formation on oral surfaces, Arch. oral Bio. 58 (2013) 1804-1811

[29] A. Kumar, A. K. Pandey, S. S. Singh, R. Shanker, A. Dhawan, Cellular uptake and mutagenic potential of metal oxide nanoparticles in bacterial cells. Chemosphere. 83 (2011) 1124–1132.

[30] S. Nagarajan, K.A. Kuppusamy, Extracellular synthesis of zinc oxide nanoparticles using seaweeds of gulf of Mannar, India. J. Nanobiotech. 11 (2013) 39.

[31] S.L. Smitha, K.M. Nissamudeen, D. Philip, K.G. Gopchandran, Studies on surface plasmon resonance and photoluminescence of silver nanoparticles, Spectrochim. Acta A (2008) 186.

[32] I.O. Sosa, C. Noguez, R.G. Barrera, Optical properties of metal nanoparticles with arbitrary Shapes, J. Phys. Chem. B 107 (2003) 6269.

[33] A. Caceres, B.R. Lopez, M.A. Giron, H. Logemann, Plants used in Guatemala for the treatment of dermatophytic infections. 1. Screening for antimycotic activity of 44 plant extracts, J. Ethnopharmacol. 31 (1991) 263-276.

[34] A. Caceres, H. Menendez, E. Mendez, E. Cohobon, B.E. Samayoa, E. Jauregui, E. Peralta, G. Carrillo, Antigonorrhoeal activity of plants used in Guatemala for the treatment of sexually transmitted diseases, J. Ethnopharmacol. 48 (1995) 85.

[35] V.K. Shukla, S. Pandey, A.C. Pandey (2010) Green synthesis of silver nanoparticles using neem leaf (*Azadirachta indica*) extract. In: Proceedings of International Conference On Advanced Nanomaterials And Nanotechnology. ICANN-2009, Guwahati, Assam (India). 9–11December (2009).

[36] N. Namratha, P.V. Monica Synthesis of silver nanoparticles using *Azadirachta indica* (Neem) extract and usage in water purification, Asian J Pharm Tech 3 (2013) 170–174.

[37] A. Lalitha, R. Subbaiya, P. Ponmurugan, Green synthesis of silver nanoparticles from leaf extract *Azhadirachta indica* and to study its anti-bacterial and antioxidant property, Int. J. Curr. Microbiol. App. Sci. 2 (2013) 228–235.

[38] Y.J. Kwon, K.H. Kim, C.S. Lim, K.B. Shim, Characterization of ZnO nanopowders synthesized by the polymerized complex method via an organo chemical route, J. Ceram. Proc. Res. 3 (2002) 146–149.

[39] R.F. Silva, M.E.D. Zaniquelli, Morphology of nanometric size particulate aluminium doped zinc oxide films, Colliods Surf. A- Physicochem. Eng. Asp. 198–200(2002) 551–558.

[40] H. Li, J. Wang, H. Liu, C. Yang, H. Xu, X. Li, H. Cui, Sol–gel preparation of transparent zinc oxide films with highly preferential crystal orientation, Vacuum 77 (2004) 57–62.

[41] H. Akiyama, K. Fujii, O. Yamasaki, T. Oono, K. Iwatsuki, Antibacterial action of several tannins against *Staphylococcus aureus*, J. Antimicrob. Chemother. 48 (2001) 487–491.

[42] M. Shelton, *Aloe vera*, its chemical and therapeutic properties. Int. J. Dermatol. 30 (1991) 679–83.

[43] V.B.K. E. Ernst *Aloe vera*: a systematic review of its clinical effectiveness. Br. J. Gen. Pract. 49 (1999) 823-8.

[44] L. Zhang, Y. Jiang, Y. Ding, M. Povey, and D. York, Investigation into the antibacterial behaviour of suspensions of ZnO nanoparticles (ZnO nanofluids). J. Nanopart. Res. 9 (2007) 479.

[45] H. Possel, H. Noack, W. Augustin, G. Keilhoff, G. Wolf, 2, 7 Dihydrodichlorofluorescein diacetate as a fluorescent marker for peroxynitrite formation. FEBS Lett. 416 (1997)175–178.

[46] H.L. Su, The disruption of bacterial membrane integrity through ROS generation induced by nano hybrids of silver and clay, Biomat. 30 (2009) 5979–5987.

[47] A.F.N.Tavares, Reactive oxygen species mediate bactericidal killing elicited by carbon monoxide-releasing molecules. J. Biol. Chem. 286 (2011) 2670–2671.

Figure Legends

Fig.1. Synthesis and surface plasmon resonance (SPR) properties of ALE-ZnONPs under varying physico-chemical conditions. The panels represent: (A) UV-Vis spectra of ALE-ZnONPs, ALE and $ZnSO_4$; (B) stability of ALE-ZnONPs based on SPR measurements up to six months (error bars represent the mean ± SE of three replicates); (C) UV-vis absorption spectra of ALE-ZnONPs synthesized under different pH (5.0, 6.0, 7.0, 8.0, 9.0 and 10.0) conditions, (D) effect of ALE concentration (10%, 20%, 30%, 40% and 50%) on ALE-ZnONPs synthesis.

Fig.2. Characterization of *A. vera* extract functionalized ALE-ZnONPs. Panel (A) depicts the X-ray diffraction pattern of ALE-ZnO-NPs, whereas panel (B) shows the FTIR spectra as (a) ALE-ZnONPs and (b) ALE alone.

Fig.3. GCMS chromatogram of phytochemicals obtained from aqeous extract of *Aloe vera leaf*. The numbers of the peaks correspond to the following compounds: 4: Ethanon 1-Phenyl, 9: Guanosine, 13: Pentadecanoic acid, 36: Tetracontane.

Fig.4. SEM, EDX, TEM and size frequency of green synthesised ALE-ZnONPs. Panel (A) shows a representative image of ALE-ZnONPs; Panel (B) represents the energy dispersive X-ray spectrum of ALE-ZnONPs; Panel (C) depicts the representative TEM image of ALE-ZnONPs and Panel (D) shows a histogram of particle size as diameter in mm.

Fig.5. Antibacterial activity of ALE-ZnONPs against multi drug resistant bacteria. Changes in absorbance, as an index of growth pattern of clinical bacterial isolates, at increasing ALE-ZnONPs concentrations and as a function of time of incubation at 37^0C, are depicted in panels (A-F). Panel (s) (A): Gram -ve (ESBL -ve) *E. coli* ATCC 25922; (B): Gram -ve (ESBL +ve); (C): Gram –ve (ESBL –ve) *P. aeruginosa* ATCC 27853; (D): Gram -ve (ESBL +ve) *P. aeruginosa* (E): Gram +ve (methicillin-sensitive) *S. aureus* ATCC 95923; and (F): Gram -ve (methicillin-resistant) *S. aureus*. The data represent the mean ± S.D of three independent experiments done in triplicate.

Fig.6. SEM photomicrographs indicating ALE-ZnONPs induced cellular damage in bacteria. Representative SEM images depict the structural deformities and cellular damage, marked by arrows in Panels (B): ESBL +ve *E. coli* cells and Panel (D): MRSA cells. The images in panels (A) and (C) show the untreated controls of *E. coli* and MRSA cells, respectively

Fig.7. Inhibition of biofilm formation by ALE-ZnONPs treated clinical isolates. Panel (A) shows the micrographs as (I): *E. coli* (ESBL +ve); (II): *P. aeruginosa* (ESBL +ve) and (III): MRSA grown in the absence (a): control, and presence of ALE-ZnONPs at varying concentrations, as (b) 500 µg/ml, (c) 1000 µg/ml) and (d) 2000 µg/ml. Panel (B) histogram showing inhibition of bacterial biofilm formation. The error bars represent mean ± S.D. of two independent experiments done in triplicates (n=6). * p value < 0.001 and * * p value < 0.05 vs control.

Fig.8. ALE-ZnONPs induced inhibition of exopolysaccharide production in *E. coli*, *P. aeruginosa* and MRSA isolates**.**

Fig.9. Flow cytometry analysis of ALE-ZnONPs interaction and internalization as a function concentration in bacteria. Panels (A) and (B) depict P1 and P2 gated population (10,000 cells) of control and treated cells of *E. coli.* and *S. aureus*, respectively, exposed to different concentrations (25, 50, 100 µg/ml) of ALE-ZnONPs for 12 h. Increase in SSC represents change in granularity due intracellular accumulation of ALE-ZnONPs, whereas increase in FSC indicates change is cell size.

Fig.10. ALE-ZnONPs induced reactive oxygen species generation in treated clinical isolates. Panel (A-I) (B-I) and (C-I) show the production of ROS in *E. coli* (ESBL +ve), *P. aeruginosa* (ESBL +ve) and MRSA respectively, exposed to different concentrations (250, 500, 1000, 2000µg/ml) of ALE-ZnONPs with ALE (10%, v/v) treated and untreated parallel controls. Panel (A-II, III, IV), (C-II, III, IV) and (C-II, III, IV) show fluorescence micrographs of unexposed and exposed bacterial cells to ALE and ALE-ZnONPs. The error bars represent mean ± S.D. of three independent experiments done in triplicates (n=6). * p value < 0.001 and * * p value < 0.05 vs control.

Fig.11. Bacterial cell viability at 10% ALE (v/v), 2000 µg/ml bulk ZnO and ALE-ZnONPs exposure against ESBL producing *E. coli, P. aeuruginosa* and methicilline resistant *S. aureus* (MRSA) clinical isolates.

Tables.

Table 1. GCMS analysis of phytocomponents present in *Aloe vera* leaf extract.

Table 2. Assessment of MIC and MBC of ALE-ZnONPs against bacterial strains.

Table 3. Quantification of intracellular Zn in bacterial cells by AAS.

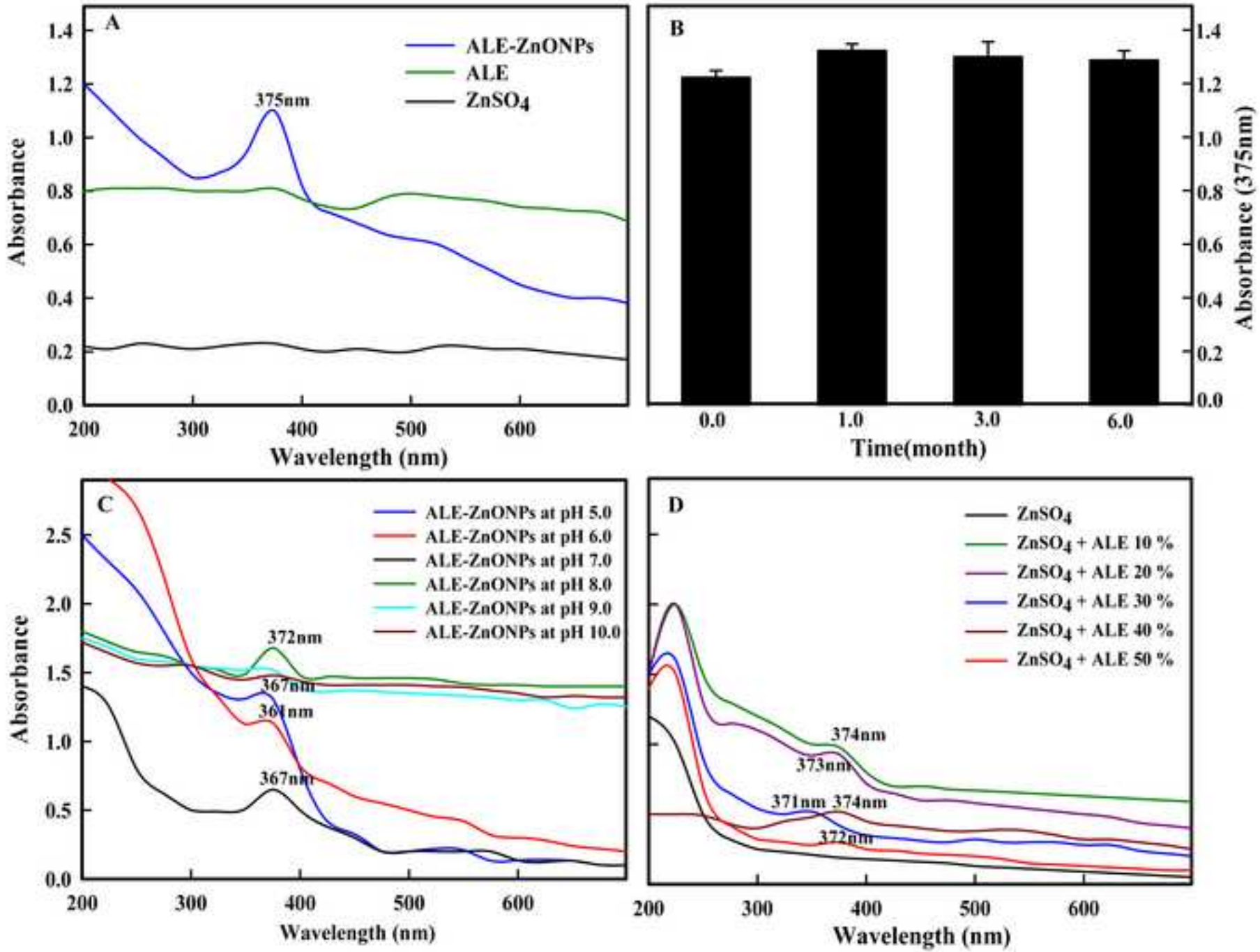

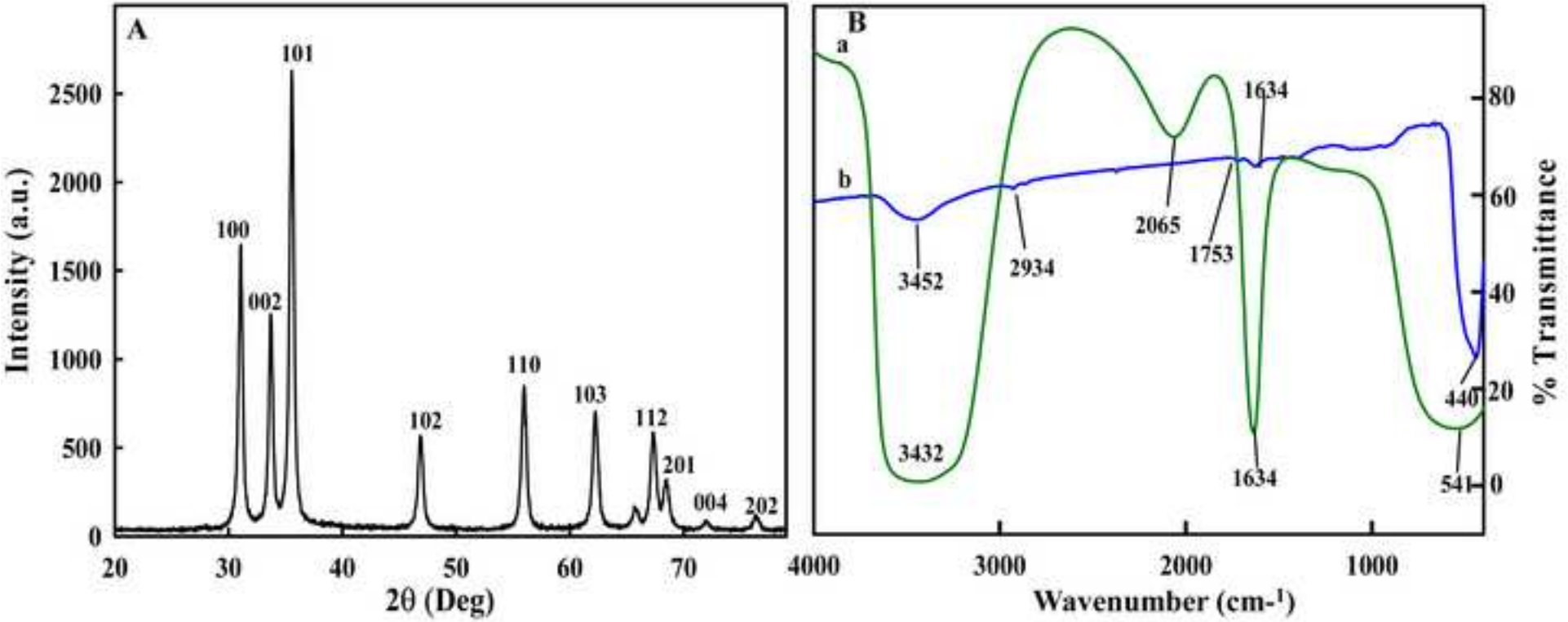

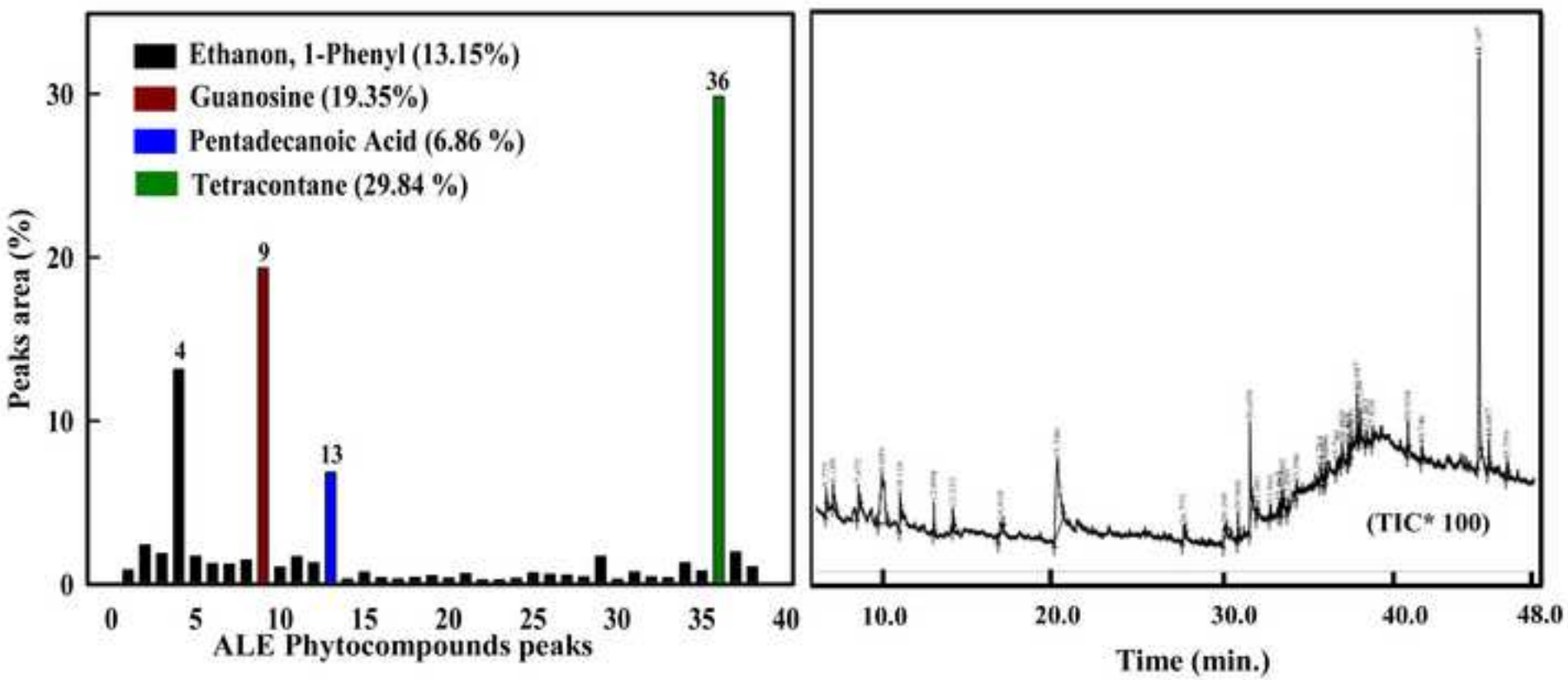

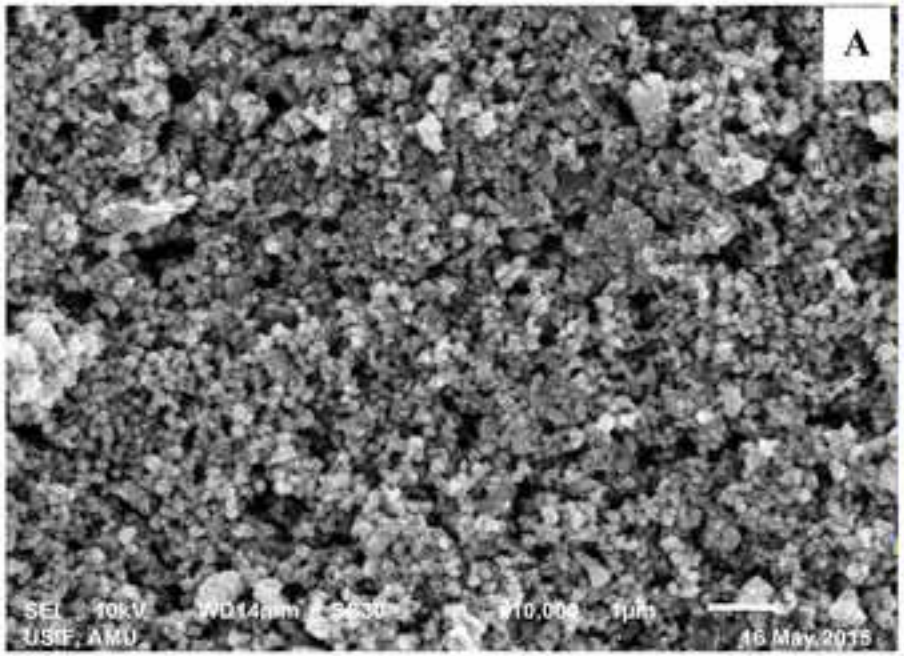

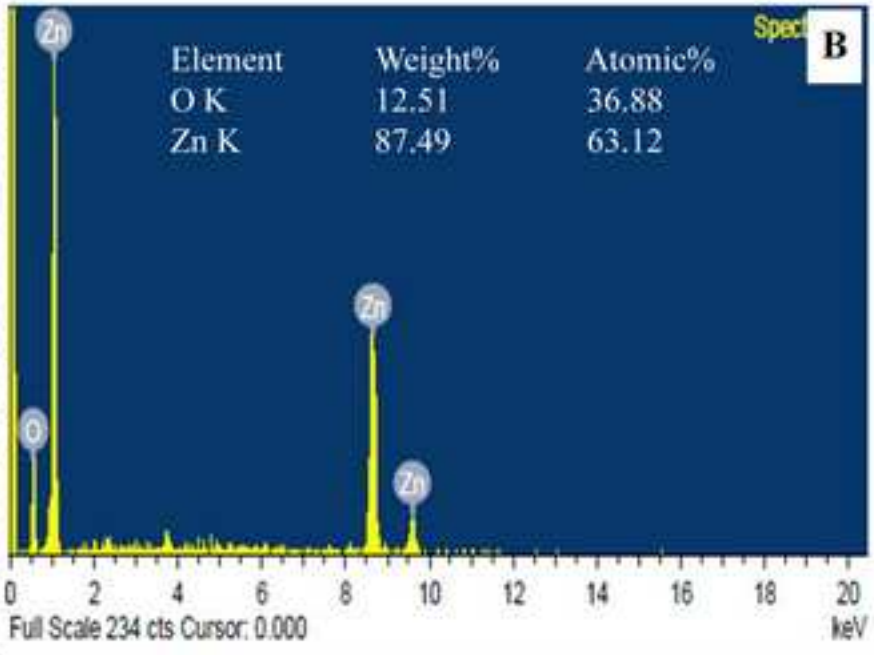

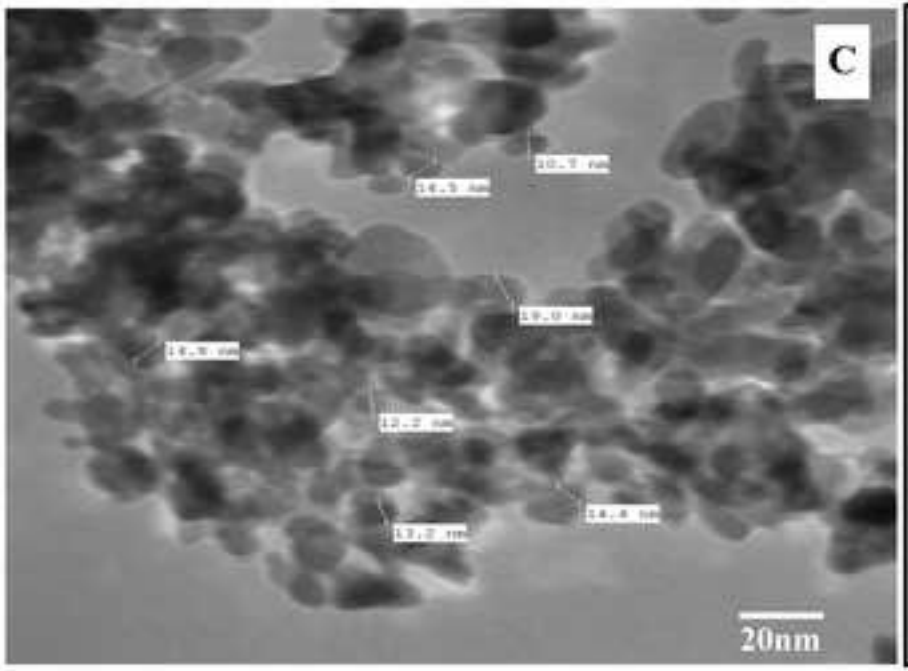

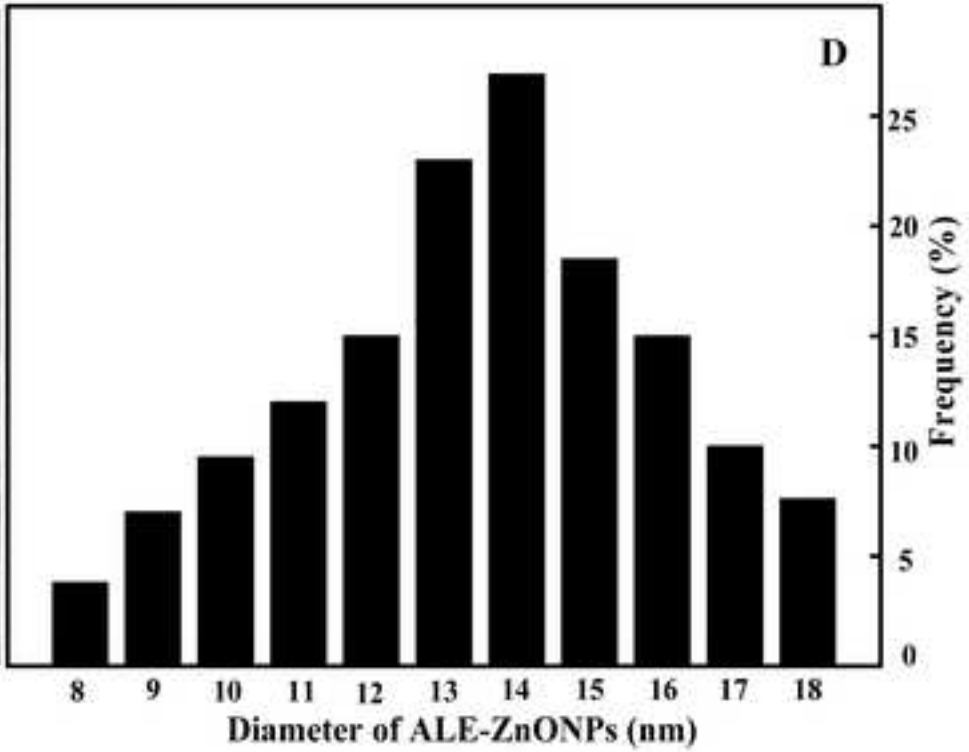

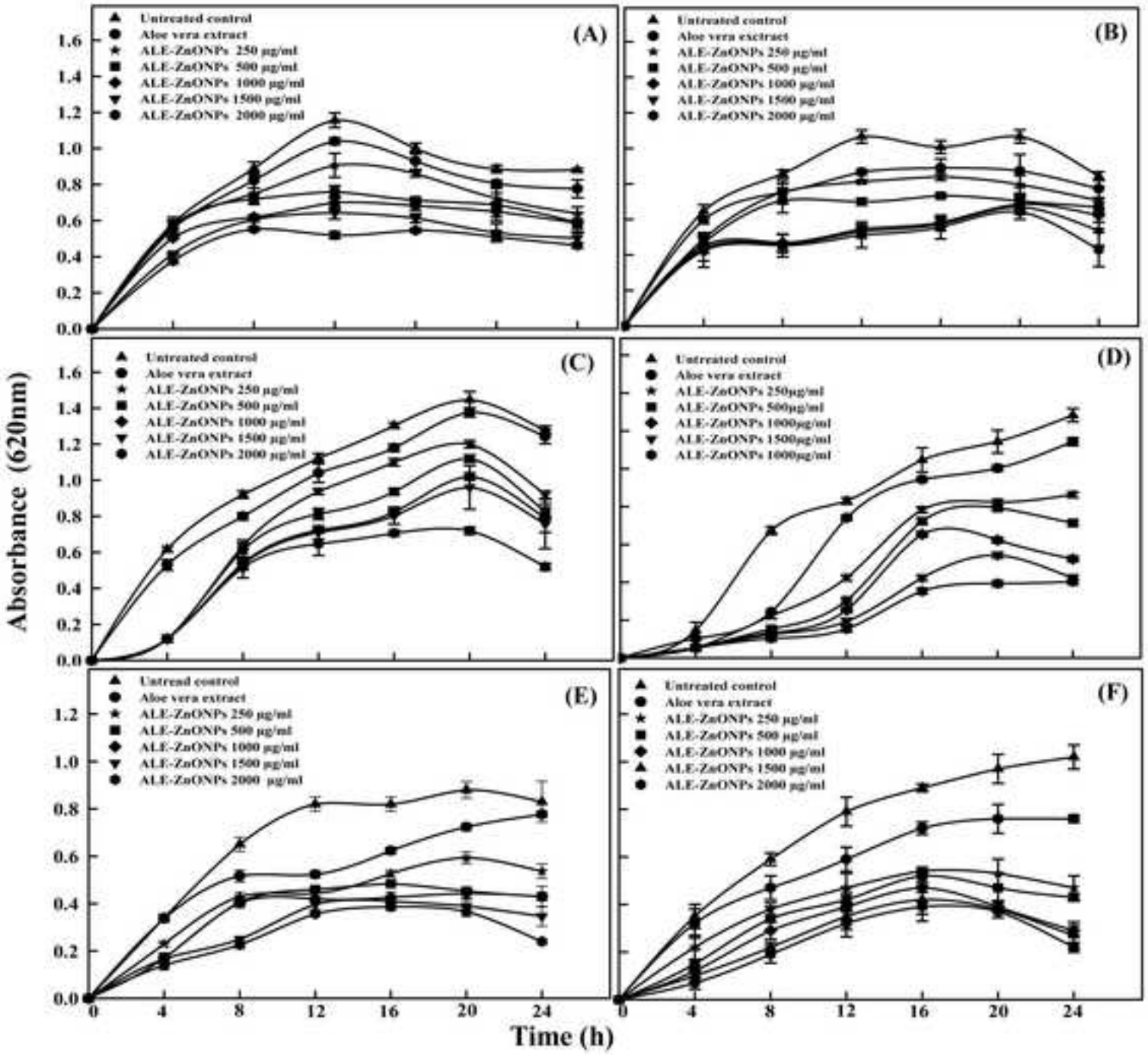

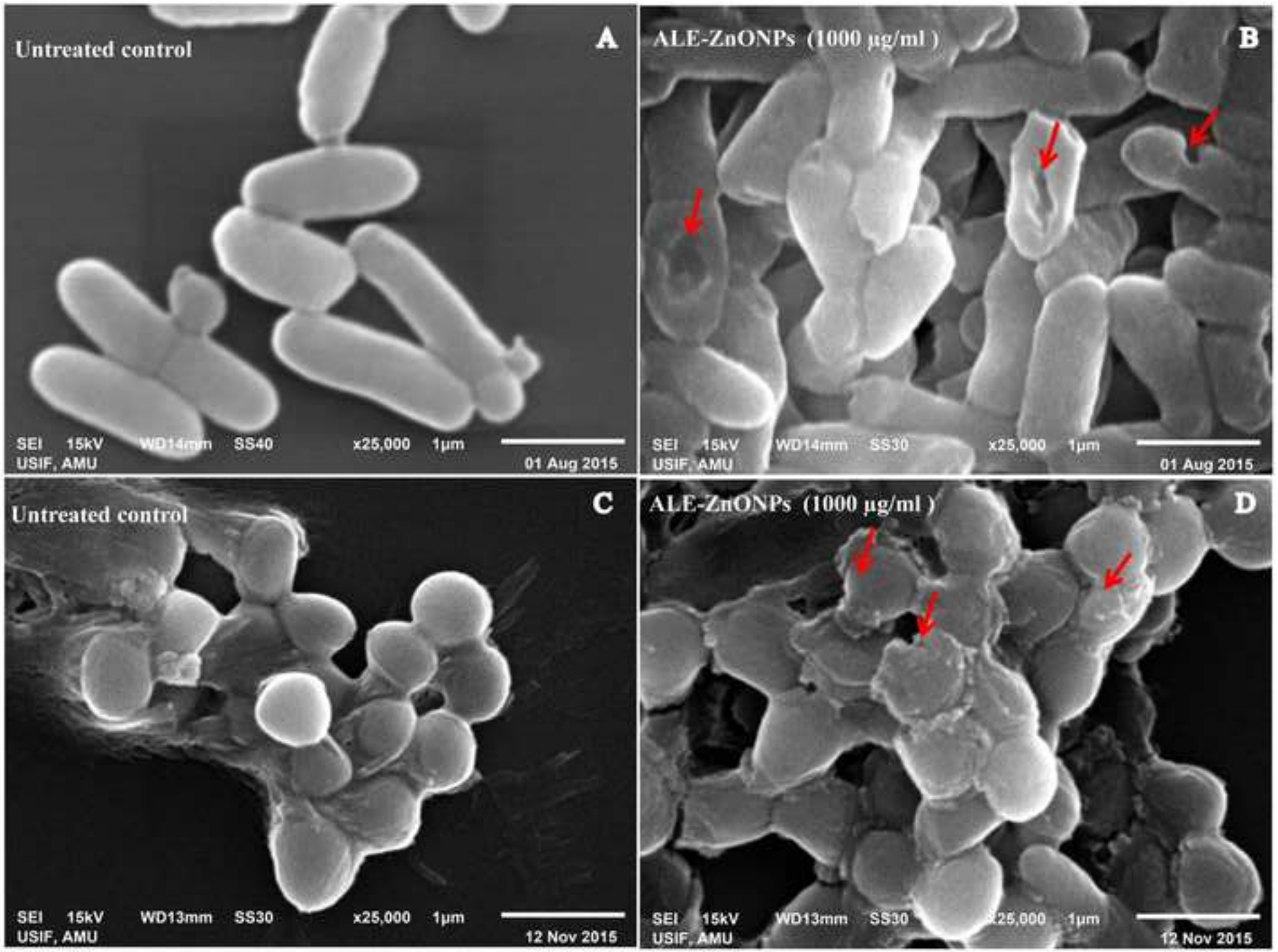

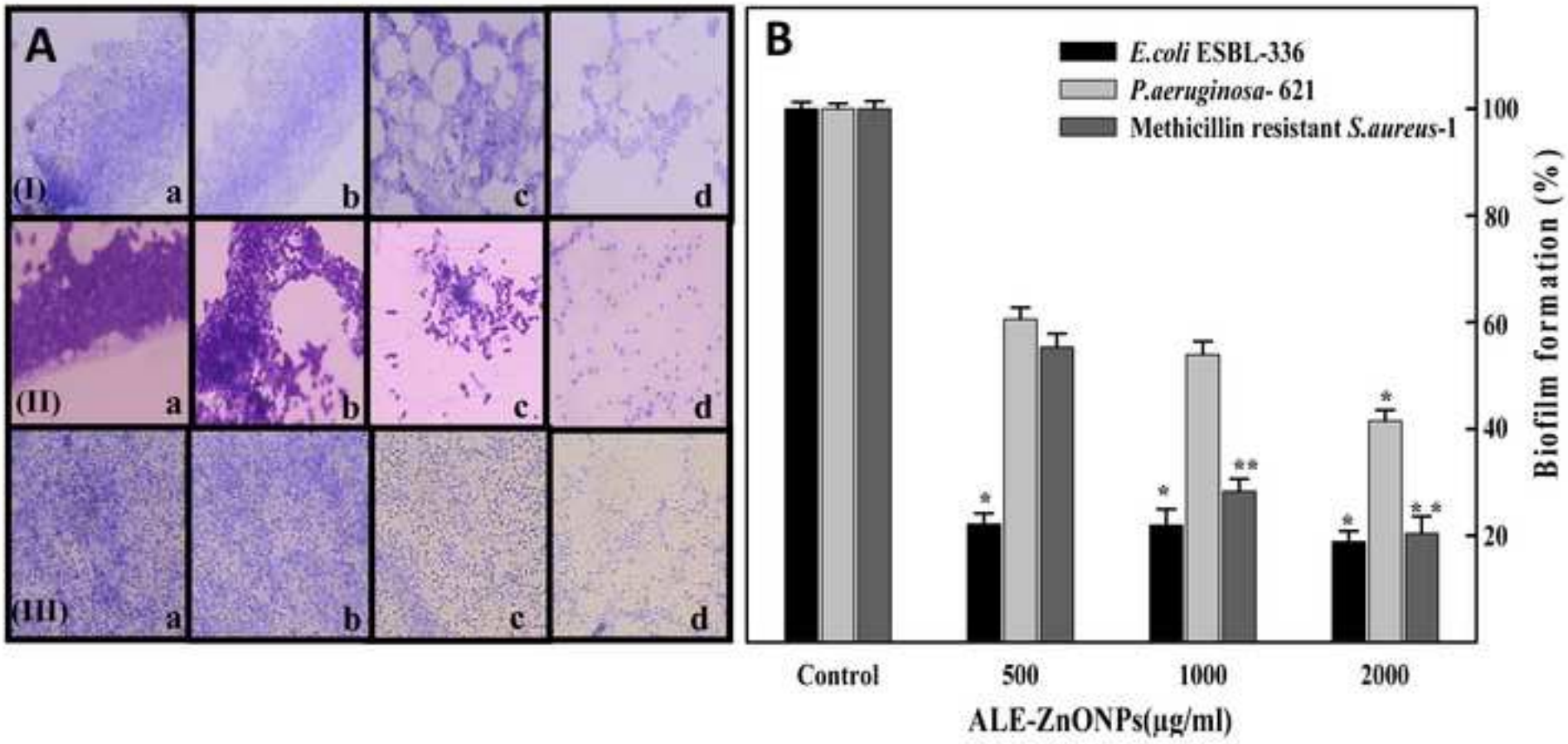

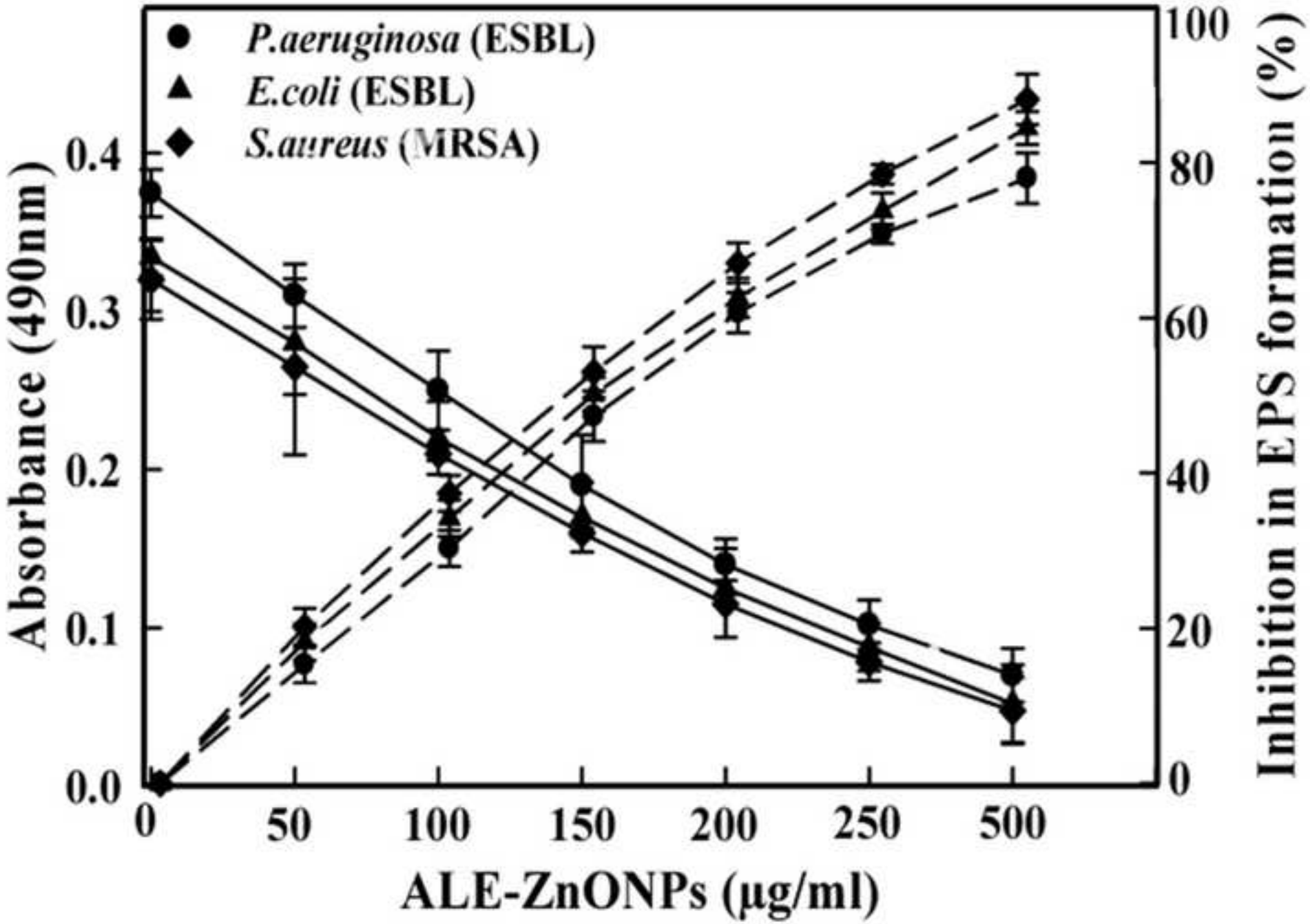

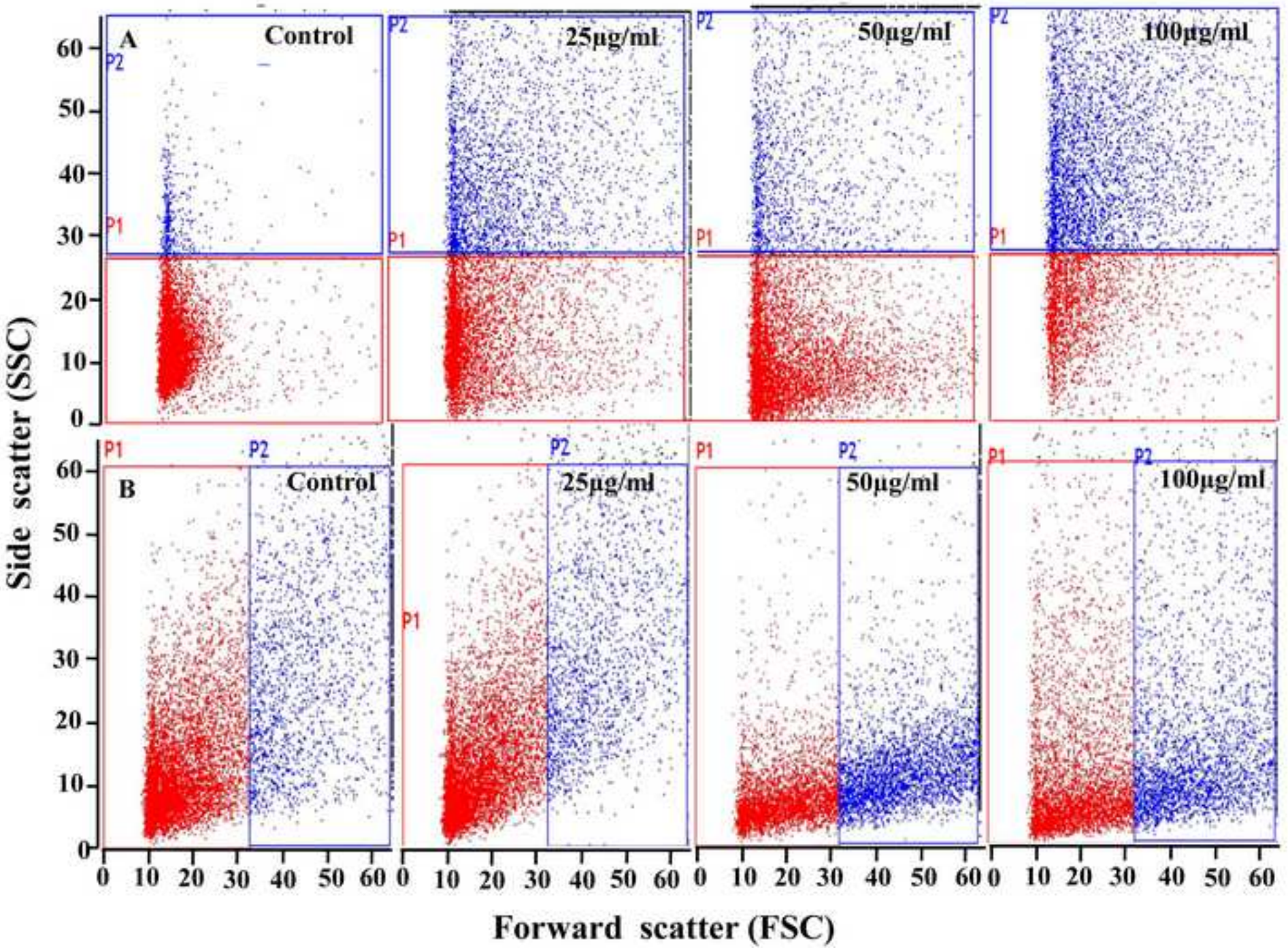

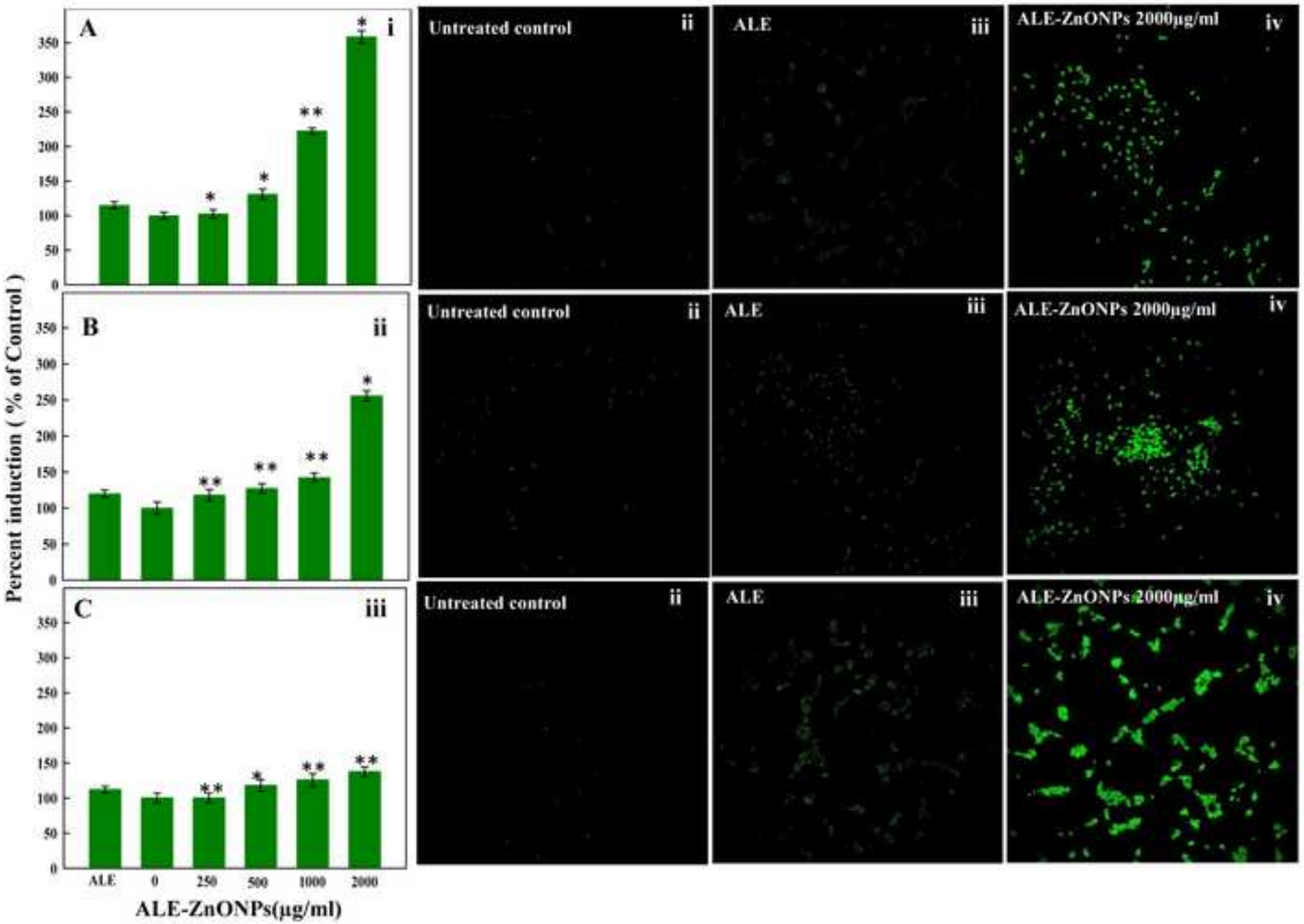

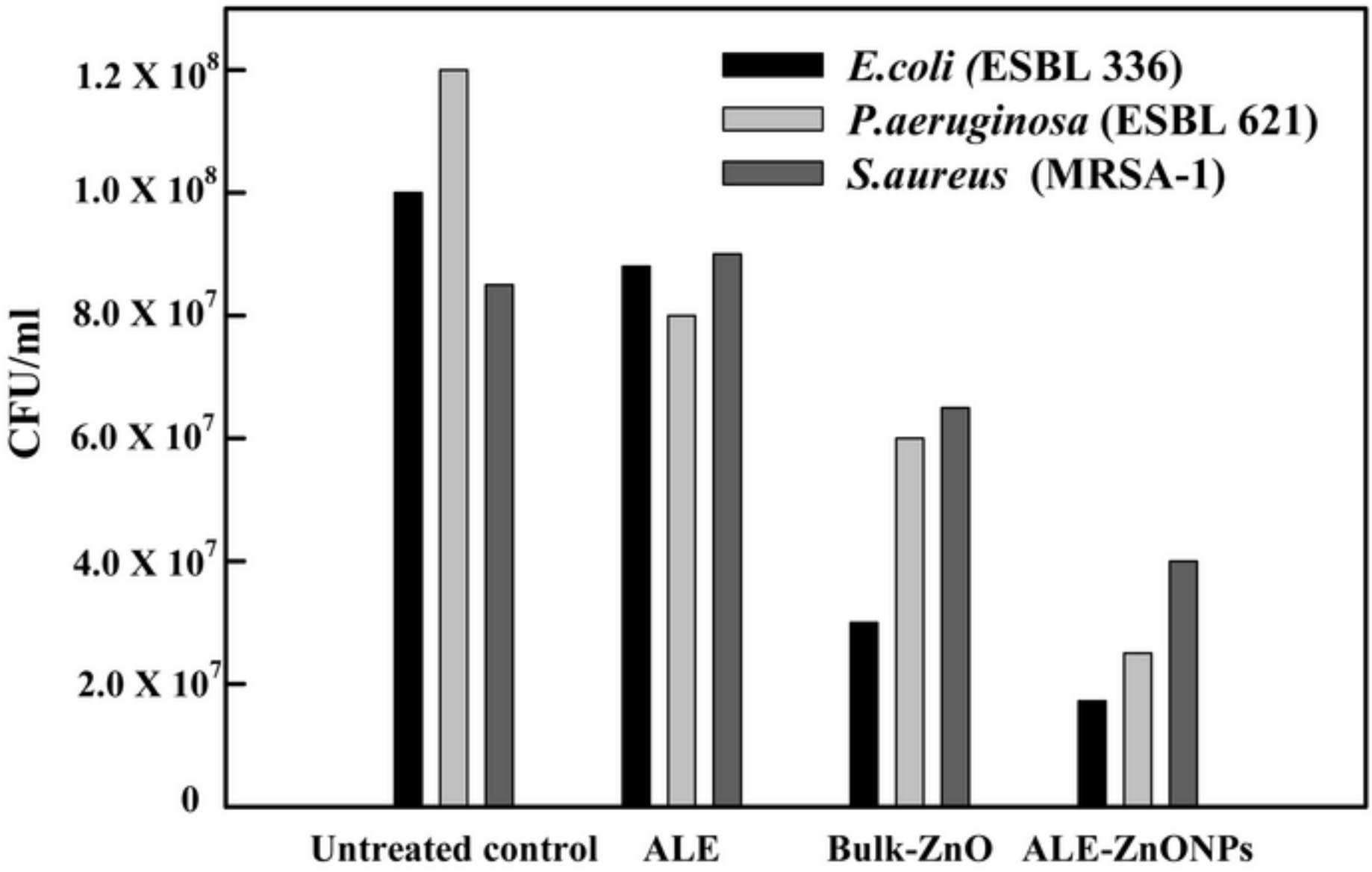

Table. 1 GCMS analysis of phytocomponents present in *Aloe vera* leaf extract

Peak	Retention Time	Peak Area%	Name of compound	Mol. Wt.	Mol. formula
1	5.775	0.88	Methoxy, Phenyl- ,Oxime	151	$C_8H_9NO_2$
2	6.189	2.41	Heptanal	114	$C_7H_{14}O$
3	7.672	1.88	2-Hydroxy-Gamma-Butyrolactone	102	$C_4H_6O_3$
4	9.059	13.15	Ethanone, 1-Phenyl	120	C_8H_8O
5	10.118	1.72	Cyclopropylmethanol	72	C_4H_8O
6	12.094	1.27	Cyclohexanol, 5-Methyl-2-(1-Methylethyl)	156	$C_{10}H_{20}O$
7	13.232	1.23	Nonanol, Trimethyl	186	$C_{12}H_{26}O$
8	16.018	1.49	2-Methoxy-4-Vinylphenol	150	$C_9H_{10}O_2$
9	19.346	19.35	Guanosine	283	$C_{10}H_{13}N_5O_5$
10	26.773	1.05	Tetradecanoic acid	228	$C_{14}H_{28}O_2$
11	29.195	1.70	2-(4-Dimethylaminostyryl)-6-phenyl-4-pyrone	317	$C_{21}H_{19}NO_2$
12	29.960	1.32	Hexadecanoic Acid, Methyl Ester	270	$C_{17}H_{34}O_2$
13	30.658	6.86	Pentadecanoic Acid	242	$C_{15}H_{30}O_2$
14	31.081	0.32	Hexadecanoic Acid, Ethyl Ester	284	$C_{18}H_{36}O_2$
15	31.861	0.75	Hexadecanoic Acid, Trimethylsilyl Ester	328	$C_{19}H_{40}O_2Si$
16	32.367	0.41	1-Octadecanol	270	$C_{18}H_{38}O$
17	32.510	0.33	9,12-Octadecadienoic Acid (Z,Z)-	280	$C_{18}H_{32}O_2$
18	32.582	0.42	9-Octadecenoic Acid (Z)-, Methyl Ester	296	$C_{19}H_{36}O_2$
19	32.895	0.53	Heptacosanoic Acid, Methyl Ester	424	$C_{28}H_{56}O_2$
20	33.396	0.38	Heptadecanoic Acid, Ethyl Ester	298	$C_{19}H_{38}O_2$
21	34.784	0.66	2-Methyltetracosane	352	$C_{25}H_{52}$
22	35.023	0.27	Sebacic Acid, Geranyl Undecyl Ester	492	$C_{31}H_{56}O_4$
23	35.096	0.27	Ethanol, 2-(9-octadecenyloxy)-, (Z)-	312	$C_{20}H_{40}O_2$
24	35.746	0.37	Tetratriacontane	478	$C_{34}H_{70}$
25	36.060	0.71	Heptadecanal	254	$C_{17}H_{34}O$
26	36.413	0.61	Butyric Acid, 4-(Benzyloxy)-, Trimethylsily	266	$C_{14}H_{22}O_3Si$
27	36.493	0.56	1,3,5-Trisilacyclohexane	132	$C_3H_{12}Si_3$
28	36.631	0.46	Tridecanol, 2-Ethyl-2-Methyl	242	$C_{16}H_{34}O$
29	36.947	1.71	Octadecanal	268	$C_{18}H_{36}O$
30	37.077	0.31	Cyclononasiloxane, Octadecamethyl	666	$C_{18}H_{54}O_9Si_9$
31	37.139	0.76	1,2-Benzenedicarboxylic Acid	390	$C_{24}H_{38}O_4$
32	37.483	0.46	Tetratetracontane	618	$C_{44}H_{90}$
33	37.838	0.40	Z-2-Octadecen-1-ol	268	$C_{18}H_{36}O$
34	39.934	1.32	Squalene	410	$C_{30}H_{50}$
35	40.746	0.81	Hexadecane, 2,6,10,14-Tetramethyl	282	$C_{20}H_{42}$
36	44.107	29.84	Tetracontane	562	$C_{40}H_{82}$
37	44.687	1.98	Stigmast-5-EN-3-OL, (3.BETA.)	414	$C_{29}H_{50}O$
38	45.759	1.07	Tritriacontane	464	$C_{33}H_{68}$
		100.00			

Table. 2 Assessment of MIC and MBC of ALE-ZnONPs against bacterial trains

	ALE-ZnONPs(µg/ml)	
Bacterial Strain	**MIC**	**MBC**
E.coli (ESBL) -336	2200	2400
E.coli- ATCC 25922	2000	2200
P. aeruginosa (ESBL)-621	2300	2700
P. aeruginosa ATCC 27853	2200	2800
S.aureus- (MRSA-1)	2000	2200
S.aureus ATCC 95923	2200	2400

Table. 3 AAS determination of Zn^{2+} in bacterial cell and growth medium

	ALE-ZnONPs(µg/ml)			
Bacterial Strain	**Zn^{2+} added**	**Zn^{2+} uptake in bacteria**	**Zn^{2+} in culture medium**	**Zn^{2+} loss**
E.coli (ESBL) -336	10,000	5897.5 (58.9%)	2390.0 (23.90%)	1712.5 (17.12%)
S.aureus - (MRSA-1)	10,000	315.0 (3.15%)	7027.5 (70.27%)	2657.0 (26.57%)

Graphical